Iranian Polymer Journal (2021) 30:355–367
https://doi.org/10.1007/s13726-020-00895-5

ORIGINAL RESEARCH

Eco-friendly polyelectrolyte nanocomposite membranes based on chitosan and sulfonated chitin nanowhiskers for fuel cell applications

Mojtaba Nasirinezhad[1] · Seyed Reza Ghaffarian[1] · Mahdi Tohidian[1]

Received: 31 August 2020 / Accepted: 21 December 2020 / Published online: 23 January 2021

Abstract
Novel sulfonic acid-functionalized chitin nanowhiskers (sChW) with enhanced proton conductivity were prepared for fabricating green and environmentally friendly chitosan (CS)-based nanocomposite polymer electrolyte membranes (PEMs). The performance of sChW in the development of direct methanol fuel cell (DMFC) nanocomposite membranes was also assessed. The manufactured nanocomposite membranes were characterized by Fourier transform infrared spectroscopy (FTIR), transmission electron microscopy (TEM), field emission scanning electron microscopy (FESEM), CHNS elemental analysis, X-ray diffractometry (XRD), ion-exchange capacity (IEC), water uptake, as well as proton conductivity and methanol permeability. The results showed that modification of chitin nanowhiskers (ChW) with sulfonic acid groups, as the proton-conducting sites, could enhance proton conductivity of the manufactured membranes, leading to a fall in methanol permeability, as a result of attractive interactions between the negatively charged sulfonic acid groups on the surface of sChW and the positively charged amine groups in the chitosan chains. Thus, the selectivity parameter (the ratio of the proton conductivity to methanol permeability) of the chitosan-based nanocomposite membranes significantly increased from 3900 for pristine chitosan PEM to 26,888 S.s.cm^{-3} (ca. 6.8 times) for a membrane with 5% (wt) sChW. The functionalization strategy used herein can pave the way for the development of efficient polyelectrolyte membranes for applications in direct methanol fuel cells.

Keywords Chitin nanowhiskers · Chitosan · Fuel cell · Methanol permeability · Proton conductivity

Introduction

In recent years, increasing concerns over the depletion of fossil fuel sources and environmental pollution have encouraged researchers and engineers to find new cost-effective and sustainable energy sources. In this regard, fuel cells have been developed as green electrical energy generation systems to directly convert the chemical energy of the fuels into electricity. Direct methanol fuel cells (DMFCs), as a member of the fuel cell family, provide several advantages, such as high energy density, simple design, low operating temperature, lightweight and ease of handling, making them an attractive energy source, especially for portable devices [1–3], medical tools [4], and also transportation sectors [5]. DMFCs can operate at ambient temperature, producing very low pollution than other vehicle emissions [6]. Polymer electrolyte membranes (PEMs), providing media for protons to be transferred between the anode and cathode sides, are considered the heart of DMFCs structures.

Because of having high proton conductivity and chemical stability, Nafion is known as a famous PEM. However, the steps taken to commercialize DMFCs were not significant due to their low efficiency at elevated temperatures or anhydrous conditions, high cost [4] as well as high methanol permeability [7]. Therefore, the development of green PEMs, as alternatives to Nafion, with high proton conductivity, low methanol permeability, excellent thermal and chemical stability, and low production costs is of great importance [8]. A big portion of related works have been focused on chitosan (CS)-based PEMs, as a natural polysaccharide with exceptional properties, such as nontoxicity, biocompatibility,

✉ Seyed Reza Ghaffarian
sr_ghaffarian@aut.ac.ir

[1] Department of Polymer Engineering and Color Technology, Amirkabir University of Technology, 15875-4413 Tehran, Iran

facile chemical functionalization, low cost, and good thermal stability [2, 9, 10]. This polymer is generally produced by the deacetylation of chitin, which is routinely obtained from the exoskeleton of crabs, shrimps, lobsters, krills, fungi, and also some kinds of insects [9, 11].

Despite several exceptional characteristics that CS enjoys, it suffers from relatively low proton conductivity in comparison to Nafion, as a consequence of its relatively high degree of crystallinity and lack of mobile protons [2, 10]. Therefore, the proton conductivity of CS can be enhanced by increasing the proportion of its amorphous structure through the addition of salts and formation of complexes, plasticization, or cross-linking [12]. Moreover, this natural polymer has a high glass transition temperature, which is characteristic of low mechanical strength leading to the brittleness of membrane [13]. In addition, having a hydrophilic nature can cause a high degree of swelling and fragility of CS-based membranes [12].

Attempts to enhance the proton conductivity of CS are not limited [2, 8, 14]. Bearing in mind the benefits of the modification of polyelectrolytes with proton-conducting sites, like sulfonic acid or imidazole groups, Xiang et al. [15] studied CS sulfate/CS blends as membranes for DMFC applications. They reported that the incorporation of CS sulfate into pure CS could cause an improvement in proton conductivity. CS also decreases methanol permeability, as a result of attractive interactions between negatively charged groups on the CS sulfate and amine groups in the pristine CS chains, which confine the free volume within the hybrid membrane. In addition, some researchers have reported the use of salt complexation of CS or doping with polyacids, which can enhance proton conductivity as well as amorphous regions in the CS structure [16]. In this regard, Soontarapa et al. [14] investigated the effect of adding lithium nitrate into cross-linked CS by sulphuric acid and achieved higher levels of proton conductivity in comparison to neat CS at 100% relative humidity (RH). Besides, blends of CS with other polyelectrolytes, such as alginate-based biopolymer [17] or polyacrylic acid [18] were studied. In this regard, Smitha et al. [19] characterized a blend of CS with poly(vinyl pyrrolidone) (PVP) for DMFC applications. They studied a semi-interpenetrating cross-linked network structure that showed an acceptable performance as a PEM for fuel cell applications.

Furthermore, as an effective strategy, incorporating proton to allow surface modification of nanofillers into CS structures seems to be an effective and feasible strategy, which not only enhances the proton conductivity through providing new sites for proton transfer but also promotes mechanical strength and thermal stability as well as decreases methanol permeability by introducing proton-conducting tortuous pathways [20, 21]. For example, it has been reported that adding proton-conducting surface functionalized nanosilica, such as sulfonated nanosilica or carboxylated ones, into CS matrix at a higher proton conductivity, as well as improved methanol barrier properties, which resulted in higher performance of the nanocomposite PEM, in comparison to the case of using the unmodified nanofillers [22]. On the other hand, it has been illustrated that the presence of phosphorylated titanate nanotube not only decreases the methanol cross over in the chitosan-based PEMs but also by providing new pathways facilitates proton transfer by P–OH groups [23].

Due to antibacterial properties, biocompatibility, biodegradability, and also low toxicity, chitin and CS are used in industrial applications, such as biomedical engineering [24], packaging [25], wastewater treatment [26], and also in cosmetics additives [27]. In the exoskeleton of crustaceans as the main source of chitin, this natural polymer forms highly crystalline microfibrils, consisting of nanofibers embedded in a protein matrix [28, 29]. Isolation of nanofibers and their conversion into rod-like nanowhiskers have been employed through various routes, such as acid hydrolysis, (2,2,6,6-tetramethylpiperidin-1-yl) oxyl (TEMPO)-mediated oxidation, wet grinding, and also ultrasonication [30]. Various applications have been mentioned for chitin nanowhiskers (ChW) as the green organic nanofillers. For instance, to increase the tensile strength of polyacrylic acid, Ofem [31] added ChW into the matrix and showed that the tensile strength of the manufactured nanocomposites increased up to 11.39%. Huang et al. [32] reported that the addition of ChW to alginate-based nanocomposite hydrogels for bone scaffold applications could significantly enhance the mechanical properties. In addition, the application of ChW in absorbing dyes with high removal efficiency has been reported elsewhere [33]. The effect of incorporating ChW into PEM structures was investigated by introducing these nanofillers in sulfonated poly(ether sulfone) (sPES). It has been shown that by adding sChW into the sPES, an enhancement in proton conductivity was achieved through the formation of long-range proton-conducting pathways as well as an improvement in the mechanical strength of the manufactured membranes [34].

To the best of our knowledge, the use of sulfonated ChW for the manufacturing of PEMs has not been reported so far. In this work, green nanocomposite membranes based on sulfonated ChW as nanofiller and CS as matrix were fabricated and characterized as a new PEM for application in DMFCs. The results were compared with those of neat CS PEM at two different temperatures. As a comparison, unmodified ChW was added to the CS matrix to depict functionalization efficiency. The proton conductivity and methanol permeability of PEMs were used to calculate the selectivity of membranes.

Experimental

Materials

Chitosan (medium molecular weight and degree of the deacetylation 80%), propane-1,3-sultone (PS), and *N*,*N*'-dicyclohexylcarbodiimide (DCC) were purchased from Sigma-Aldrich (USA). Acetic acid, hydrochloric acid, sodium hydroxide, ethanol, tetrahydrofuran (THF), acetonitrile, sodium hydroxide, and sodium chloride were all purchased from Merck (USA). All materials were used without further purification. Shrimp waste (catching from the Persian Gulf) was obtained from the local market.

Preparation and purification of chitin

For purification of chitin, in the first step, all the meat and soft tissues were separated, and hard shells were washed with tap water several times. Then the shells were dried for 72 h and ground. The obtained powder was passed through a stainless steel mesh (No 50 mesh) until a homogeneous powder was obtained. The chitin extraction was done in three steps, namely demineralization, deproteinization, and decolorization [35]. The powder was added to 5% (wt) hydrochloric acid to dissolve all minerals for 24 h at room temperature. Then, the mixture was filtered and washed with distilled water several times. The resulted powder was treated with a 5% (wt) sodium hydroxide solution (1:20 *w*:*v*) to remove the existing proteins for 12 h at 65 °C. Afterward, this mixture was filtered and washed with distilled water several times to reach a neutral pH. In the next step, acetone was used for decolorization of the obtained powder for 12 h at room temperature. The final powder was washed with distilled water and dried in a vacuum oven at 65 °C for subsequent uses.

Preparation of chitin nanowhiskers

The acid hydrolysis method, with minor modifications, was used for the extraction of ChW from chitin powder in this work [36]. Briefly, 5 g of chitin powder was refluxed with 150 mL 3 N hydrochloric acid at 95 °C for 90 min. The supernatant was separated by centrifugation at 4000 rpm, and the residuals were treated again with 3 N hydrochloric acid two further times. After the final treatment, for neutralization and removing the remaining impurities, a 12 k Dalton dialysis tube in distilled water was used. The distilled water was refreshed every 8 h until pH 6 was achieved. Finally, the suspension was freeze-dried to obtain solid water-free sChW for subsequent uses.

Surface modification of ChW

To modify the surface of sChW with sulfonic acid groups, 1 g of freeze-dried sChW was added to THF and stirred for 12 h, and then homogenized with ultrasonication for a total of 30 min. Then, 1.5 g of propane-1,3-sultone, as well as 2.5 g of DCC were added to the mixture at 70 °C under vigorous stirring for 36 h. In the next step, the resulting sChW were separated by centrifugation and filtration. To remove any residual reactants, THF Soxhlet was used for 6 h, and then, the substantial part was washed with acetonitrile several times, and finally, the product was freeze-dried for further uses.

Membranes preparation

Dried CS powder was dissolved in an acetic acid aqueous solution (1% (*v*:*v*)) to preparea 1% (*w*:*v*) solution. To fabricate the nanocomposite membranes containing 1, 3, 5, and 7% (wt) of the modified nanofillers, appropriate amounts sChW were ultrasonicated in dilute acid aqueous solutions for 30 min, and the resultant mixtures were added into the CS solutions, respectively. Then, the homogenous mixtures were poured into the leveled glass Petri-dishes and incubated at 25 °C for 3 days, and then dried at 60 °C for 6 h in a vacuum oven. The dried membranes were neutralized with 5% (wt) sodium hydroxide solution and washed with distilled water several times until neutral pH was achieved. Afterward, the membranes were cross-linked with 0.5 M sulfuric acid solution for 24 h at room temperature. Finally, the membranes were washed with distilled water to remove physically absorbed acid and stored in distilled water until subsequent uses. The manufactured membranes were generally named as CHx that x denotes the loading weight of sChW within the membrane. Another CS membrane containing 5% (wt) of ChW (named CHU) was prepared with the same procedure, as mentioned above. Figure 1 shows the procedure of fabricating the nanocomposite membranes.

Characterization

Fourier transform infrared (FTIR) spectroscopy

To ensure the functionalization of sChW, the FTIR spectra of the nanofillers (4000–450 cm^{-1}, resolution 2 cm^{-1}) were recorded by a Perkin Elmer Fourier transform infrared spectrometer (Spectrum 65), using KBr tablets.

Elemental analysis

To evaluate the quantity of sulfuric acid groups functionalized on the surface of sChW, the elemental analysis was performed with a CHNS-O Elemental Analyzer instrument

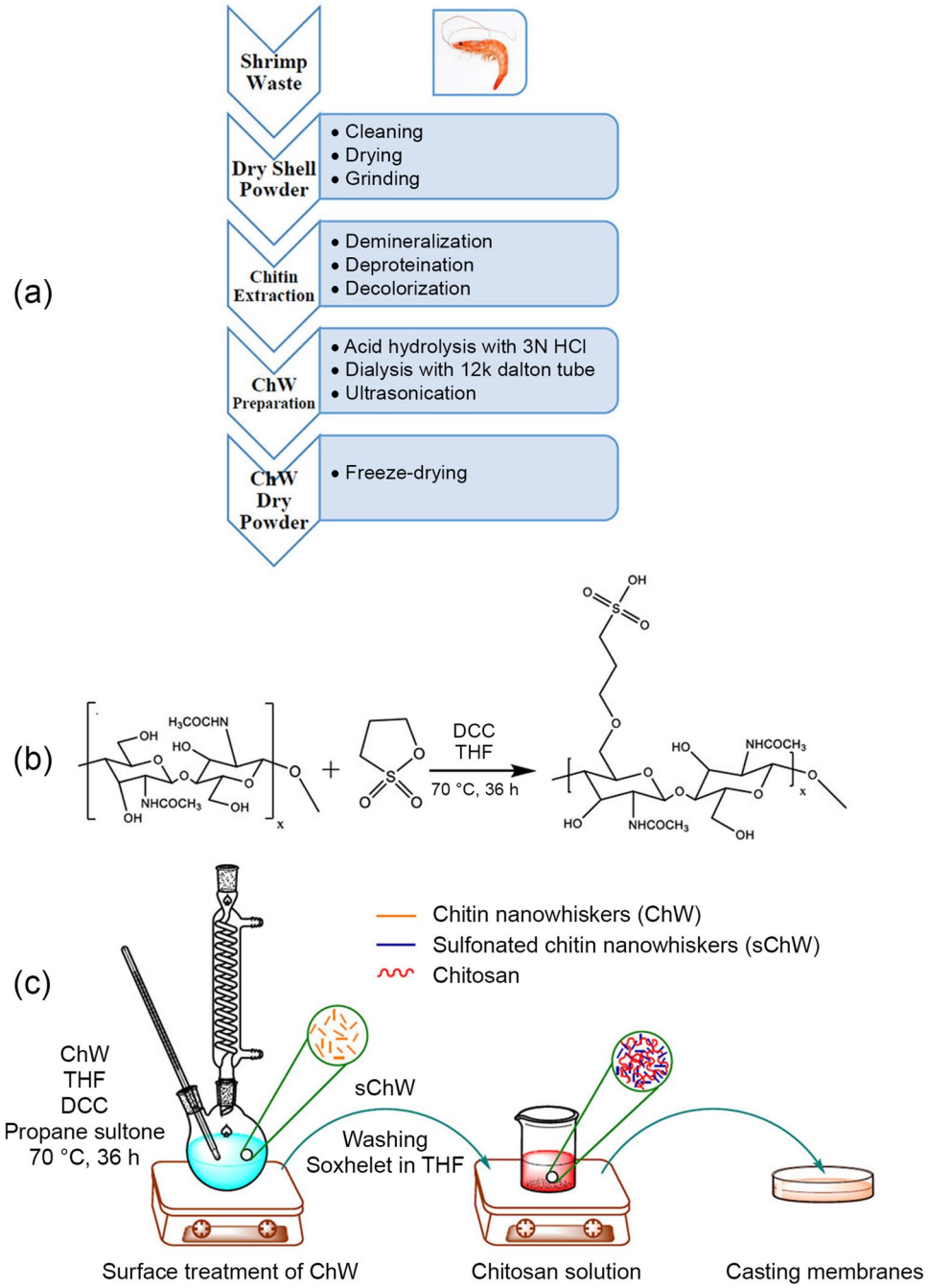

Fig. 1 **a** Preparation process of ChW, **b** the synthesis route of sChW, **c** schematic illustration procedure for fabricating the nanocomposite membranes

(model ECS 4010, Costech Analytical Technologies Inc., Italy).

X-ray diffraction

X-ray diffraction (XRD) patterns were utilized to investigate the crystalline structure of ChW or sChW. In this regard, 50 mg of each sample was analyzed by a Philips X-ray diffractometer (PW1730 Model, Philips Co., Netherland), which was equipped with Cu K_α tube operating at 40 kV, 30 mA. To calculate the crystalline index (CI) of ChW, as well as sChW, Eq. 1 was applied, which was proposed by Zhang et al. [37]:

$$\mathrm{CI} = \frac{I_{110} - I_{\mathrm{am}}}{I_{110}} \times 100, \tag{1}$$

where, I_{110} is the intensity of diffraction peak at 19.5° and I_{am} is the minimum intensity at the amorphous region between 2θ of 9.5° (I_{020}) and 2θ of 19.5° (I_{110}). Also, the d-spacing of the crystalline structures was determined by the Bragg's equation [38] (Eq. 2):

$$d = \frac{\lambda}{2\sin\theta}, \tag{2}$$

where, λ is the wavelength of X-ray (1.540 Å), and θ is the angle of diffraction. The average crystallite size was calculated by the Debye–Scherrer equation (Eq. 3):

$$\mathrm{DI}_{110} = \frac{0.9\lambda}{\beta\cos\theta}, \tag{3}$$

where, β is the full width at half maximum (FWHM) in radians, θ is the Bragg diffraction angle of the 110 peak at 2θ of 19.5°, and λ is the wavelength of X-ray (1.540 Å).

Microscopic assessments

To observe the shape and size of the nanowhiskers in aqueous suspension, transmission electron microscopy (TEM) (Model CM120, Philips, Netherland) was implemented. For this purpose, a dilute aqueous dispersion of sChW (0.01% by wt) was prepared. Also, the field emission scanning electron microscopy (FE-SEM) technique was used for investigating the morphology of cross section of the dried nanocomposites, which were fractured in liquid nitrogen. In this regard, TESCAN MIRA III (Czech) device was utilized.

Thermal gravimetric analysis (TGA)

Thermal stability of ChW and sChW, as well as their manufactured nanocomposite membranes, was examined by a DSC/TGA analyzer (TA, Q600, USA) from 25 to 600 °C at the rate of 10 °C/min under the nitrogen atmosphere.

Water uptake

As the water content has a significant role in the proton conduction mechanisms through the PEMs, investigating the water uptake behavior of these membranes seems essential. Hence, the dried samples were immersed in deionized water, and then, at various times, after removing the surface water with tissue paper, the membranes were weighed quickly until no further weight gain was observed. The amount of water uptake was calculated based on Eq. 4**,** where W_w and W_d are the weights of the membrane in the wet and dry states, respectively.

$$\mathrm{WU}(\%) = \frac{W_w - W_d}{W_w}. \tag{4}$$

Ion-exchange capacity (IEC)

To determine the IEC values of the CS membrane, all the dried samples were weighed and immersed in a 100 mL 1 M sodium chloride solution to replace H^+ with Na^+ ions. The obtained solution was titrated with 0.01 M sodium hydroxide standard solution with phenolphthalein indicator. The IEC values were calculated using Eq. 5:

$$\mathrm{IEC} = \frac{V \times C}{m}, \tag{5}$$

where, V is the volume in mL and C is the concentration of sodium hydroxide solution in mol/L used to neutralize the obtained previous solution, and m is the weight of the dried membrane.

Proton conductivity

To evaluate the proton conductivity of the membranes, the electrochemical impedance spectroscopy (EIS) technique was employed with an Autolab PGstat 303 N potentiostat/galvanostat impedance analyzer (Echochemie) with the 4-Probe method in the frequency range 0.1 Hz–100 kHz with the signal amplitude 5 mV. Before testing, the membranes were hydrated in deionized water for 48 h. The electrical resistivity of the membranes was determined from the intercept of high-frequency impedance. The proton conductivity of the membranes was obtained from Eq. 6:

$$\sigma = \frac{L}{R \times A}, \tag{6}$$

where, σ is the proton conductivity (S/cm^2), L is the thickness (cm), R is the electrical resistivity (S^{-1}) obtained from EIS graphs, and A is the lateral surface (cm^2) of the specimen.

Methanol permeability

As the barrier properties of PEMs against methanol play a significant role in the overall efficiency of DMFCs, the methanol permeability of the membranes was measured by a laboratory diffusion cell consisting of two reservoirs. One of these reservoirs was filled with distilled water (cell A), and the other one was filled with 2 M aqueous methanol solution (cell B). A mixer was stirred continuously in cell A and cell B to ensure homogeneity. The methanol concentration in cell A was measured at different time intervals by the refractometry method [39, 40], using ATAGO Abbe refractometer. The methanol permeability of the membranes was calculated using Eq. 7:

$$P = \frac{1}{C_B} \times \frac{\Delta C_A(t)}{\Delta t} \times \frac{V_A \times L}{A}. \tag{7}$$

In this respect, C_B is the concentration of methanol (mol/L) in cell B, $\frac{\Delta C_A(t)}{\Delta t}$ is the slope of methanol concentration graph at different time intervals in cell A (mol/s), V_A

is the volume of each reservoirs (cm^3), L is the membrane thickness (cm), *A* is the membrane surface area (cm^2), and *P* is the methanol permeability of each membrane (cm^2/s).

Results and discussion

The electrochemical properties of PEMs are affected by incorporating the nanofillers within their structure. Such an effect is rooted in changes in the concentration of proton-conducting sites and introducing new pathways for the protons to be transferred through the membranes [16, 41]. Because of playing an effective role in the proton-conducting mechanisms, resulting in an enhancement in the proton conductivity, sulfonic acid groups are known as attractive sites to be immobilized on the surface of the nanofillers, resulting in an enhancement in the overall efficiency of the cells. In this regard, the surface of ChW was modified by functionalizing $–SO_3H$ groups and afterward introduced into CS-based nanocomposite membranes to provide new PEMs for DMFCs applications.

Characterization of nanowhiskers

The FTIR spectra of ChW, as well as sChW, are depicted in Fig. 2. As can be seen, the peaks at 1561, 1621, and 1654 cm^{-1} are assumed as typical characteristics bands of chitin, which are attributed to the amide I and amide II groups in ChW, as well as sChW [34]. The peaks around 1100 cm^{-1} are ascribed to the glycosidic linkage in the pyranose ring in the chitin structure [42], which is overlapped on the etheric bond in the case of sChW, as a result of the reaction between the hydroxyl groups in ChW and propane-1,3-sultone. In the case of sChW, the peaks in this region have more intensity in comparison to ChW. Such an effect is also evident in the regions around 2884 cm^{-1} and 2934 cm^{-1} that are ascribed to the methylene groups in ChW and sChW, which is attributed to the presence of more methylene groups in the structure of sChW, as a result of $–SO_3H$ functionalization on the surface. Finally, in the case of sChW, the characteristic band of S–O–S (around 1370 cm^{-1}) is overlapped on the absorption peak of methyl groups in acetyl groups, present in the chitin-based structures [42]; however, the mentioned peaks in this region are more intensified, which can be attributed to the functionalization of $–SO_3H$ groups on the surface of sChW.

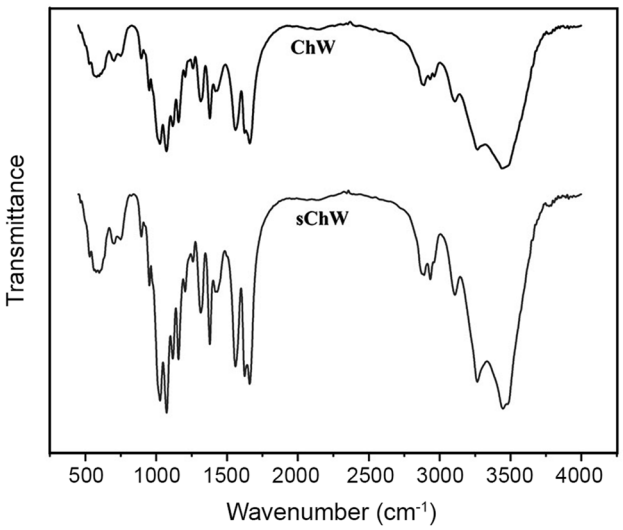

Fig. 2 FTIR spectra of ChW, and sChW in the range of 4000–450 cm^{-1}

Table 1 illustrates the results of the CHNS test, which was applied to ensure the successful surface modification of sChW. The results indicated the existence of sulfur in sChW samples that is due to the successful surface modification of sChW with sulfonic acid groups.

Furthermore, the increase in the carbon content and the decrease in nitrogen elemental content in sChw, compared to ChW, can be ascribed to the successful functionalization of $–SO_3H$ groups as a result of the reaction between PS and –OH groups in chitin.

The XRD patterns of ChW, as well as sChW are depicted in Fig. 3. As shown, the characteristics diffraction peaks of both ChW and sChW, which were observed at around 2θ of 9.5°, 19.5°, 20.8°, 23.4°, and 26.6° could correspond to the 020, 110, 120, 101, and 130 planes, respectively [37]; however, the intensity of the peaks in sChW has been diminished. This observation might be attributed to a decrease in the crystallinity of sChW, in comparison to Chw, as a result of the modification of the nanowhiskers, which caused changes in the surface structure and, as a consequence, the level of crystallinity in these nanofillers and also crystallite sizes. The chemical modification affects the crystallinity of this polymer. Hai and Sugimoto [43] showed that the crystallinity index (CI) of chitin was dropped by functionalization with poly(3-hexylthiophene) (P3HT), but XRD typical peaks of chitin appeared at around 9.5°, 19.5°, and 23° associated with the 020, 110, and 130 planes observed in the modified chitin, respectively. Li et al. [44], who studied the chitin nanocrystals grafted with L-lactide, showed that such functionalization could reduce the CI value. The crystallite

Table 1 CHNS elemental analysis of ChW and sChW

Sample	C (% by wt)	N (% by wt)	H (% by wt)	S (% by wt)
ChW	44.78	6.24	7.02	Not detected
sChW	46.41	6.04	7.23	0.94

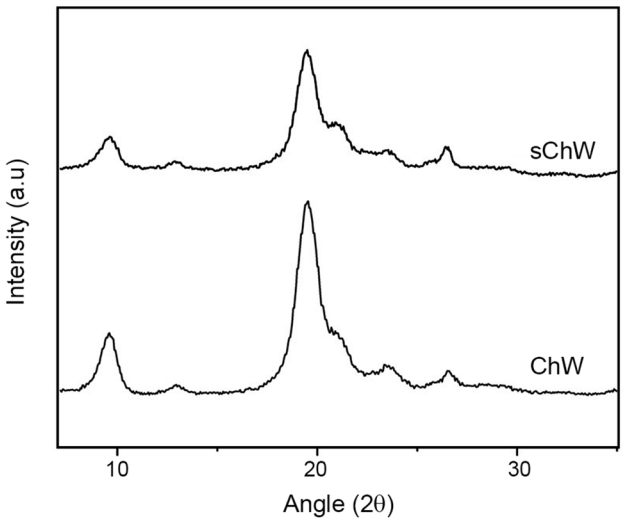

Fig. 3 XRD patterns of sChW in comparison to ChW

size was slightly decreased, suggesting that the crystalline structure was preserved in the modified chitin nanocrystals. It was also reported that alkali treatment of chitin can deteriorate crystallinity until it reaches a plateau [45]. Table 2 shows the values of crystalline index (CI), *d*-spacing and crystallite size for ChW and sChW calculated by Eqs. 1–3, respectively.

Microscopic assessments

Figure 4 shows the TEM image of the dried dilute ChW suspension (0.01% by wt). A rod-like structure with the average diameter of 15–30 nm and length of 150–300 nm was observed, indicating that the nanowhiskers have a relatively broad size distribution. In addition, the FESEM images of ChW and sChW are illustrated in Fig. 5. These images show that although the fibrillary structure is preserved in sChW, the surface of the nanowhiskers becomes coarser after the modification with sulfonic acid groups. This observation is in agreement with the XRD results.

Table 2 Crystalline index (CI), *d*-spacing and crystallite size of ChW and sChW

Sample	CI (%)	$2\theta^{o}$	*d*-spacing (Å)	Crystallite size at (110) plane (Å)
ChW	94.6	9.60	9.20	44
		12.9	6.85	
		19.55	4.53	
		20.70	4.29	
		23.40	3.80	
		26.50	3.36	
sChW	90.6	9.65	9.16	31
		13.00	6.81	
		19.50	4.55	
		20.75	4.28	
		23.55	3.77	
		26.40	3.37	

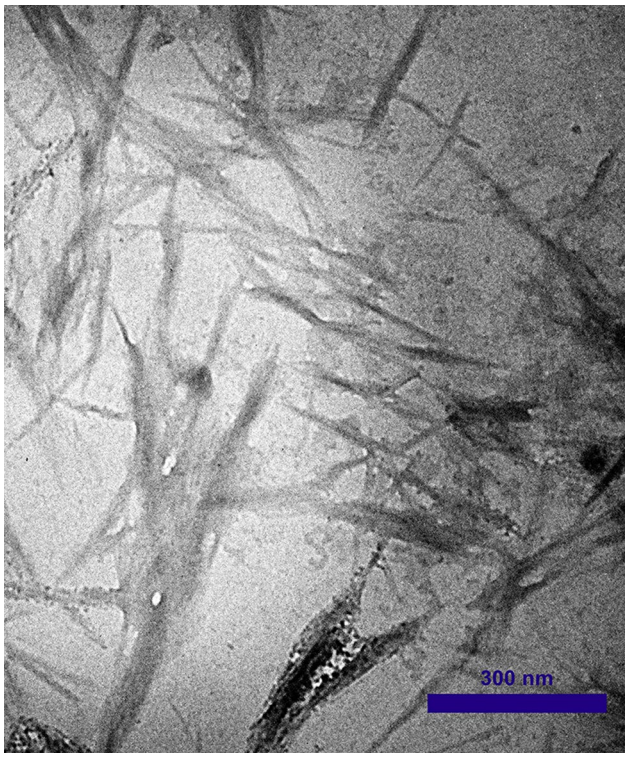

Fig. 4 TEM image of ChW

Figure 6 shows the fractured cryogenic surface of CH0, CHU, and CH5. According to these pictures, CS PEM illustrates a relatively dense and homogeneous cryogenic fractured surface with no apparent cracks or defects. Moreover, it can be found that unlike CHU, in the case of CH5, there are no significant pinholes, which is related to the pulling out of the nanowhiskers. Such phenomena may be rooted in strong interfacial interactions between sChW and the CS matrix. We believe that the surface modification of sChW caused attractive interactions between the CS matrix and the surface of the nanofiller, which resulted in a stronger interface.

Thermal behavior

The thermal degradation behaviors of ChW and sChW are shown in Fig. 7a. The degradation of ChW showed two stages involving weight loss of about 100 °C due to moisture absorption and subsequent decomposition of the chitin skeleton at higher temperatures. As it is obvious, the degradation onset temperature of sChw occurred at a slightly lower temperature, compared to that of ChW, which is ascribed to the

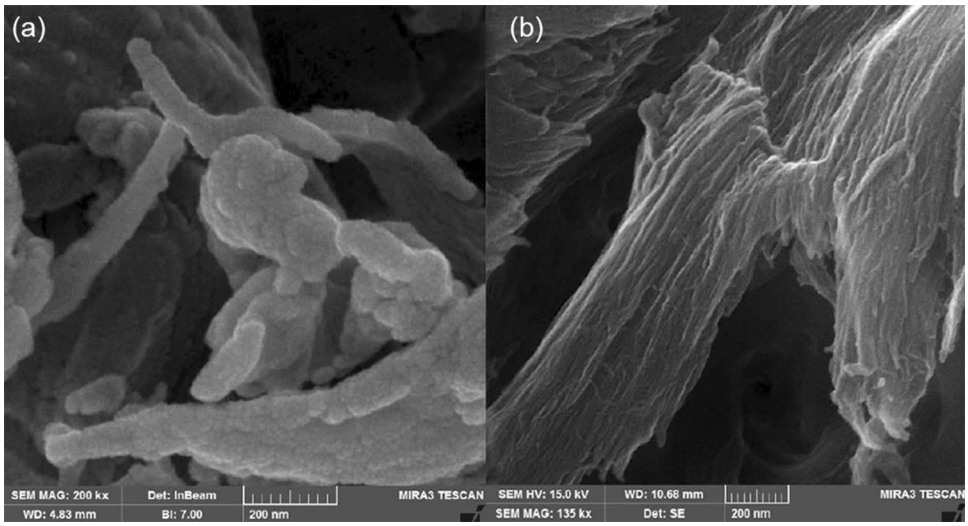

Fig. 5 FESEM images of **a** ChW, and **b** sChW

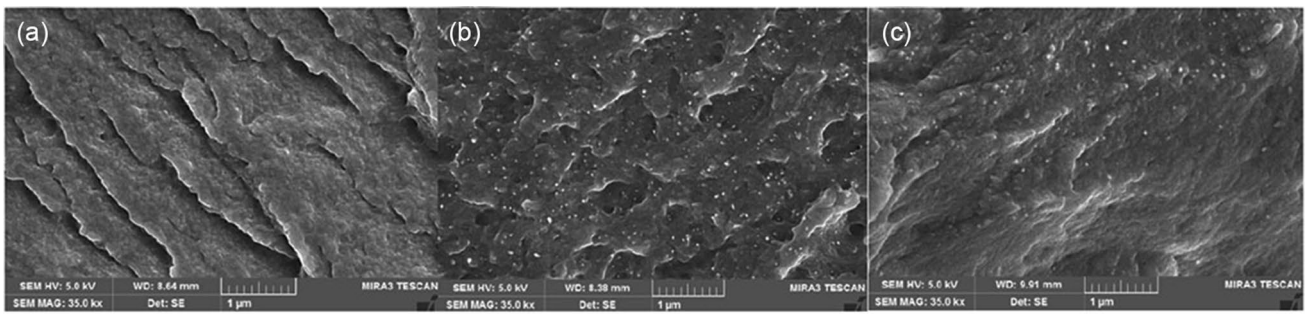

Fig. 6 FESEM images of the nanocomposite membranes, **a** CH0, **b** CHU, and **c** CH5

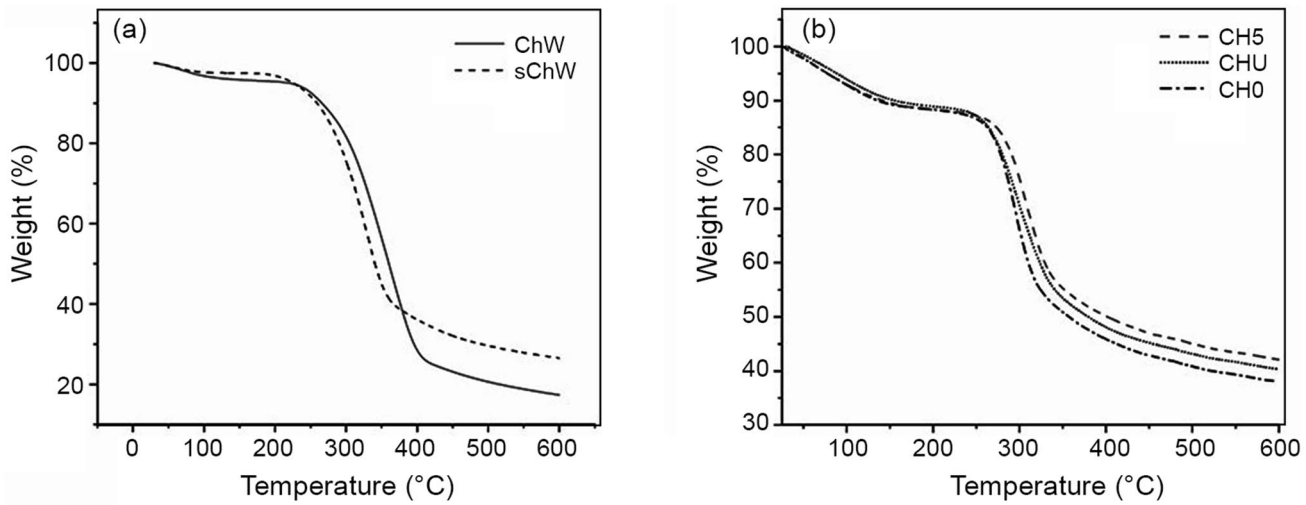

Fig. 7 Thermal decomposition behavior of: **a** ChW and sChW, and **b** CH0, CH5, and CHU as a function of temperature

degradation of sulfonic acid groups, functionalized on the surface of sChW between 190 and 250 °C [46]. Furthermore, the decomposition step of the chitin skeleton occurred at 368 °C and 331 °C for ChW and sChW, respectively, which can be attributed to a reduction in the degree of crystallinity in sChW in comparison to ChW [46]. In addition, the

residual mass amount after heating up to 600 °C was 17.21% (wt) for ChW, while it was 26.42% (wt) for sChW, which is in agreement with the previous reports [47]. The catalytic role of sulfonic groups in dehydration of chitin structure can cause higher char residue in sChW compared to ChW. Similar to what has been reported about sulfated cellulose [48, 49], it can be assumed that the presence of sulfonic acid groups in the structure of sChW is able to catalyze the extraction of water from the structure of chitin at temperatures above 100 °C. Since the produced water molecules can immediately evaporate at elevated temperatures, the presence of carbon atoms resulting from carbon monoxide or carbon dioxide is very unlikely; instead, they remain as char and increase the residual mass.

Figure 7b illustrates the thermal degradation behavior of CH0, CH5, and CHU membranes. As expected, the onsets of decomposition slightly increased for the nanocomposite membranes containing sChW or ChW as the nanofillers. Higher thermal stability in CH5, in comparison to CHU, may be rooted in attractive interfacial interactions, such as electrostatic interactions or hydrogen bonding between the surface of sChW and CS chains [2].

Characterization of PEMs

Water molecules have a crucial role in the performance of PEMs since they can act as proton carriers within the membrane; however, the excessive water content can result in weakening the mechanical properties [13]. In this regard, the water uptake of the studied membranes was determined three times, and the average values are presented in Table 3. As can be seen, the water uptake of CHU and all the membranes containing different loading weights of sChW are lower than that of CH0. This behavior can be ascribed to the packed crystalline structure of chitin-based nanowhiskers introduced into membranes, which results in lower water absorption compared to CS PEM [50, 51]. Similar phenomena are reported by Li et al., who studied the membranes composed of CS as the matrix and cellulose nanowhiskers (CW) [52] as the nanofiller. Furthermore, it was observed that with an increase in the content of sChW within the nanocomposite membranes, the water uptake values were decreased. This behavior, due to the lower water uptake in CHU, compared to CH5, is attributed to attractive electrostatic interactions between the surface of modified nanowhiskers and the CSmatrix.

IEC values, which represent the numbers of exchangeable ion sites in one gram of the prepared membranes, can affect the proton conductivity of PEMs. According to the results listed in Table 3, with an increase in the content of sChW within the fabricated nanocomposite membranes, the IEC values were increased, which can be related to the existence of sulfonic acid groups as the ion-exchange sites, functionalized on the surface of sChW. In this regard, the IEC value in CH7 was measured 30% higher than that in CS PEM (CH0). Shirdast et al. reported similar results and studied CS-based nanocomposite membranes incorporated with sulfonated graphene oxides [2]. Furthermore, it should be noticed that the pristine CSIEC values were improved through cross-linking by sulfuric acid [14]. Finally, the reduced IEC values of CHU, compared to CH0, could be associated with a lower number of proton-conducting sites in Chw.

Generally speaking, vehicle and Grotthuss (hopping) are known as the major mechanisms for proton diffusion within the PEMs. In the vehicle mechanism, free water molecules play a role in transferring the protons as hydronium ions; however, Grotthuss-type diffusion is related to the proton hopping from one proton-conducting site to another one through hydrogen bonding networks [16]. Proton conductivities of all the samples were determined at room temperature and the results are shown in Table 3. Consistent with IEC results, all nanocomposite membranes containing sChw showed higher proton conductivity in comparison to CS PEM, which is due to an enhancement in concentration

Table 3 Water uptake, IEC, proton conductivity, methanol permeability and selectivity parameter values of the nanocomposite membranes at room temperature and 100% relative humidity

Sample	Water uptake (wt%)	IEC (mmol/g)	Proton conductivity (S/cm)	Methanol permeability (cm^2/s)	Selectivity parameter (Ss/cm^3)
CH0	78.9 ± 0.4	0.65 ± 0.01	0.0039 ± 0.0001	$1E-6$	3900
CHU	76.1 ± 0.4	0.60 ± 0.02	0.0036 ± 0.0001	$5.8E-7$	6207
CH1	77.2 ± 0.5	0.68 ± 0.02	0.0066 ± 0.0003	$9.2E-7$	7174
CH3	72.6 ± 0.4	0.77 ± 0.02	0.0078 ± 0.0004	$7.2E-7$	10,833
CH5	68.7 ± 0.3	0.83 ± 0.01	0.0121 ± 0.0009	$4.5E-7$	26,888
CH7	66.2 ± 0.5	0.91 ± 0.01	0.0179 ± 0.0012	$8.7E-7$	20,574
CS/P(AA-AMPS)-(H2SO4)	–	–	0.0036	$2.41E-7$	14896 [57]
Sulfonated CS	–	–	0.0145	$4.7E-7$	30851 [15]

of proton-conducting sites through incorporating sulfonic acid-functionalized nanowhiskers and an improvement in proton transfer through the hopping mechanism [2]. Incorporating Chw in the CHU nanomembrane caused a slight reduction in the proton conductivity, which might be related to a decrease in water absorption, and especially introducing tortuous proton-conducting pathways. In this regard, Tohidian et al. [53] showed that by introducing nanosilica at high loading weights to Nafion-based nanocomposites, the proton conductivity is decreased due to lower water uptake and the hindrance of free proton conduction through masking the proton-conducting sites.

Table 4 shows the proton conductivity of all samples at 65 °C. For all the studied samples, the proton conductivity was increased with an increase in the temperature, which is due to an enhancement in the diffusivity of hydronium ions through the membranes [54, 55]. Figure 8 suggests a mechanism for the presumptive proton-conducting tortuous pathways. The interactions between $–SO_3H$ groups grafted on the surface of sChW and the H^+ mainly enhance the proton hopping (Grotthuss-type) mechanism of proton conduction and correspondingly the overall performance of the fuel cell membranes. Incorporating sChW into the chitosan PEM increases the proportion of the proton-conducting sites within the nanocomposite membrane with respect to the chitosan PEM, which facilitates proton transport. In addition, the positively charged chains of chitosan are electrostatically cross-linked by the adsorbed sulfuric acid groups acting as new proton-conducting sites promoting the proton conductivity, especially through proton hopping mechanism.

Table 4 Proton conductivity, methanol permeability and selectivity parameter of the membranes at 65 °C and 100% relative humidity

Sample	Proton conductivity (S/cm)	Methanol permeability ($\times 10^{-6}$ cm^2/s)	Selectivity parameter (Ss/cm^3)
CH0	0.0080 ± 0.0004	2.30 ± 0.09	3478 ± 233
CH1	0.0131 ± 0.0005	1.94 ± 0.08	6753 ± 405
CH3	0.0147 ± 0.0007	1.37 ± 0.06	10,730 ± 665
CH5	0.0194 ± 0.0009	0.93 ± 0.05	20,860 ± 968
CH7	0.0221 ± 0.0013	1.58 ± 0.06	13,987 ± 867

Since the fuel permeability through the PEMs can cause a reduction in the efficiency of DMFCs, some strategies have been applied to decrease the permeability of methanol through the PEMs, such as introducing nanofillers within the membranes and producing more tortuous diffusion pathways [56]. The methanol permeabilities of all the samples were evaluated and the results are depicted in Table 3. In agreement with the water uptake behavior of the studied membranes, the methanol permeability decreased with an increase in the loading weights of sChW up to 5% (wt) within the membranes, which is attributed to a reduction in the membranes free volumes, as a result of the attractive interactions between amine groups in the CS chains and sulfonic acid groups grafted on the surface of sChW, as well as introducing tortuous diffusion pathways. We have previously reported such phenomenon in Nafion-based PEMs, that by adding imidazole functionalized carbon nanotube, the methanol permeability of those nanocomposite membranes was reduced, as a result of the electrostatic interactions between positively charged imidazole rings on the surface of imidazole functionalized multi-walled carbon nanotubes (MWCNTs) and sulfonic acid groups in Nafionas the matrix

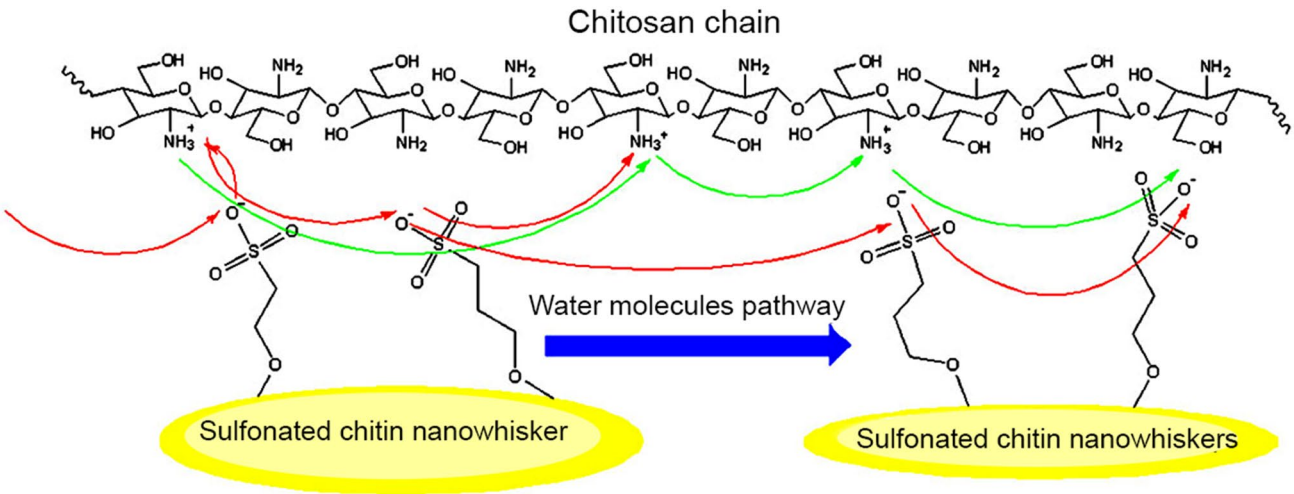

Fig. 8 Schematic of the proton-conducting pathways through the chitosan nanocomposite membranes containing sulfonic acid-functionalized nanowhiskers

[54]. On the other hand, with an increase in the content of sChW in CH7, compared to CH5, the methanol permeability increased, which might be related to the agglomerations of the nanowhiskers in the nanocomposites and the increment of nanovoids as free routs for methanol diffusion. Finally, in the case of CHU, the values of methanol permeability were higher than those of CH5, which is due to the role of electrostatic interactions between the surface of modified nanofiller and the matrix, and also a reduction in the free volume of those containing sChW.

The methanol permeability of the membranes was also determined at 65 °C (Table 4). The methanol permeability at higher temperature was increased for all the samples, which is due to the easier penetration of methanol molecules at the higher temperatures. We previously observed such behavior in the case of CS PEMs filled with different types of organically modified nanoclays [16].

As both the proton conductivity and the methanol permeability simultaneously affect the DMFC performance, the membrane selectivity parameter, defined as the ratio of proton conductivity (desirable) to methanol permeability (undesirable), is normally considered to choose the optimal PEMs for practical DMFC applications. In this regard, Tables 3 and 4 show the selectivity parameter of all the manufactured membranes at 25 and 65 °C, which determine the efficiency of the membranes in DMFC structures. For all nanocomposite samples, the selectivity parameters were higher than those for CS PEM. Among all the studied samples, the CH5 showed the highest selectivity parameter. Such an observation could be attributed to the better formation of nanofiller/polymer matrix interface, which led to the fewer formation of nanovoids at the interface and, as a result, lower methanol permeability, along with relatively high proton conductivity as a consequence of introducing more proton-conducting sites within the membrane. In this regard, and based on the obtained results, CS nanocomposite membranes containing 5% (wt) sChW are proposed as efficient and eco-friendly membranes for DMFC applications.

Conclusion

To introduce new polymer electrolyte membranes (PEMs) for fuel cell applications, a series of nanocomposite membranes were prepared and characterized by incorporation of sulfonic acid-functionalized chitin nanowhiskers into the CS matrix. The infrared spectroscopy and the elemental analysis demonstrated the successful surface modification of the nanowhiskers by the reaction between propane-1,3-sultone and –OH groups in chitin nanowhiskers (named as sChW). The X-ray diffraction patterns showed that the crystalline structure was preserved in the chemically modified nanowhiskers. In addition, all the studied nanocomposite membranes showed higher proton conductivity, in comparison to the CSPEM, without any nanofiller content, which was attributed to the role of functionalized groups on the surface of modified nanowhiskers in the proton conduction mechanisms. Furthermore, the fabricated nanocomposite membranes showed lower levels of methanol permeability as a result of attractive interactions between the surface of incorporated modified nanofillers and the matrix, which resulted in higher values of the selectivity parameter for the fabricated nanocomposite PEMs. Accordingly, the nanocomposite membranes based on CS and sulfonic acid-functionalized chitin nanowhiskers can be considered as potential PEMs for DMFC applications.

Acknowledgements The authors thank Mr. J. Jafari from Sahand University of Technology for helpful fundamental discussions. This research was supported by Amirkabir University of Technology, Tehran, Iran.

References

1. Bashir S, Liu JL (2015) Advanced nanomaterials and their applications in renewable energy. Elsiver, Amsterdam
2. Shirdast A, Sharif A, Abdollahi M (2016) Effect of the incorporation of sulfonated chitosan/sulfonated graphene oxide on the proton conductivity of chitosan membranes. J Power Sources 306:541–551
3. Tohidian M, Ghaffarian SR, Shakeri SE, Bahlakeh G (2013) Sulfonated aromatic polymers and organically modified montmorillonite nanocomposite membranes for fuel cells applications. J Macromol Sci B 52:1578–1590
4. Mukoma P, Jooste B, Vosloo H (2004) A comparison of methanol permeability in Chitosan and Nafion 117 membranes at high to medium methanol concentrations. J Membr Sci 243:293–299
5. Tenson TJ, Baby R (2017) Recent advances in proton exchange membrane fuel cells: a view. Int Adv Res J Sci Eng Tech 4(6):34–40
6. Singh D, Lu D, Djilali N (1999) A two-dimensional analysis of mass transport in proton exchange membrane fuel cells. Int J Eng Sci 37:431–452
7. Zakaria Z, Kamarudin SK, Timmiati S (2016) Membranes for direct ethanol fuel cells: an overview. Appl Energy 163:334–342
8. Shakeri SE, Ghaffarian SR, Tohidian M, Bahlakeh G, Taranejoo S (2013) Polyelectrolyte nanocomposite membranes, based on chitosan-phosphotungstic acid complex and montmorillonite for fuel cells applications. J Macromol Sci B 52:1226–1241
9. Osifo PO, Masala A (2012) The influence of chitosan membrane properties for direct methanol fuel cell applications. J Fuel Cell Sci Technol 9:011003–011012
10. Ramadhan L, Radiman C, Suendo V, Wahyuningrum D, Valiyaveettil S (2012) Synthesis and characterization of polyelectrolyte complex *N*-succinylchitosan-chitosan for proton exchange membranes. Procedia Chem 4:114–122
11. Ifuku S, Saimoto H (2012) Chitin nanofibers: preparations, modifications, and applications. Nanoscale 4:3308–3318
12. Vaghari H, Jafarizadeh-Malmiri H, Berenjian A, Anarjan N (2013) Recent advances in application of chitosan in fuel cells. Sustain Chem Process 1:16
13. Rosli NAH, Loh KS, Wong WY, Yunus RM, Lee TK, Ahmad A, Chong ST (2020) Review of chitosan-based polymers as proton

exchange membranes and roles of chitosan-supported ionic liquids. Int J MolSci 21:632
14. Soontarapa K, Intra U (2006) Chitosan-based fuel cell membranes. Chem Eng Commun 193:855–868
15. Xiang Y, Yang M, Guo Z, Cui Z (2009) Alternatively chitosan sulfate blending membrane as methanol-blocking polymer electrolyte membrane for direct methanol fuel cell. J Membr Sci 337:318–323
16. Tohidian M, Ghaffarian SR, Shakeri SE, Dashtimoghadam E, Hasani-Sadrabadi MM (2013) Organically modified montmorillonite and chitosan–phosphotungstic acid complex nanocomposites as high performance membranes for fuel cell applications. J Solid State Electrochem 17:2123–2137
17. Shaari N, Kamarudin S (2015) Chitosan and alginate types of biomembrane in fuel cell application: an overview. J Power Sources 289:71–80
18. Smitha B, Sridhar S, Khan A (2004) Polyelectrolyte complexes of chitosan and poly (acrylic acid) as proton exchange membranes for fuel cells. Macromolecules 37:2233–2239
19. Smitha B, Sridhar S, Khan A (2006) Chitosan–poly (vinyl pyrrolidone) blends as membranes for direct methanol fuel cell applications. J Power Sources 159:846–854
20. Tripathi BP, Shahi VK (2011) Organic–inorganic nanocomposite polymer electrolyte membranes for fuel cell applications. Prog Polym Sci 36:945–979
21. Ma J, Sahai Y (2013) Chitosan biopolymer for fuel cell applications. Carbohydr Polym 92:955–975
22. Wang J, Zhang H, Jiang Z, Yang X, Xiao L (2009) Tuning the performance of direct methanol fuel cell membranes by embedding multifunctional inorganic submicrospheres into polymer matrix. J Power Sources 188:64–74
23. Wang J, Zhao Y, Hou W, Geng J, Xiao L, Wu H, Jiang Z (2010) Simultaneously enhanced methanol barrier and proton conductive properties of phosphorylated titanate nanotubes embedded nanocomposite membranes. J Power Sources 195:1015–1023
24. Mohebbi S, Nezhad MN, Zarrintaj P, Jafari SH, Gholizadeh SS, Saeb MR, Mozafari M (2019) Chitosan in biomedical engineering: a critical review. Curr Stem Cell Res Ther 14:93–116
25. Rinaudo M (2006) Chitin and chitosan: properties and applications. Prog Polym Sci 31:603–632
26. Prashanth KH, Tharanathan R (2007) Chitin/chitosan: modifications and their unlimited application potential: an overview. Trends Food Sci Technol 18:117–131
27. Jimtaisong A, Saewan N (2014) Utilization of carboxymethyl chitosan in cosmetics. Int JCosmet Sci 36:12–21
28. Li M-C, Wu Q, Song K, Cheng H, Suzuki S, Lei T (2016) Chitin nanofibers as reinforcing and antimicrobial agents in carboxymethyl cellulose films: influence of partial deacetylation. ACS Sustain Chem Eng 4:4385–4395
29. Raabe D, Al-Sawalmih A, Yi S, Fabritius H (2007) Preferred crystallographic texture of α-chitin as a microscopic and macroscopic design principle of the exoskeleton of the lobster Homarus americanus. Acta Biomater 3:882–895
30. Salaberria AM, Labidi J, Fernandes SC (2015) Different routes to turn chitin into stunning nano-objects. Eur Polym J 68:503–515
31. Ofem MI (2017) Characterisation of alpha-chitin/poly (acrylic acid) blend films. Mater Discovery 9:1–10
32. Huang Y, Yao M, Zheng X, Liang X, Su X, Zhang Y, Lu A, Zhang L (2015) Effects of chitin whiskers on physical properties and osteoblast culture of alginate based nanocomposite hydrogels. Biomacromol 16:3499–3507
33. Meshkat SS, Nezhad MN, Bazmi MR (2019) Investigation of Carmine dye removal by green chitin nanowhiskers adsorbent. Emerg Sci J 3:187–194
34. Zhang C, Zhuang X, Li X, Wang W, Cheng B, Kang W, Cai Z, Li M (2016) Chitin nanowhisker-supported sulfonated poly (ether sulfone) proton exchange for fuel cell applications. Carbohydr Polym 140:195–201
35. Pighinelli L, Broquá J, Zanin B, Zanin B, Flach A, Mallmann C, Taborda F, Machado L, Alves S, Silva M (2019) Methods of chitin production a short review. Am J Biomed Sci Res 3:307–314
36. Pereira AG, Muniz EC, Hsieh YL (2014) Chitosan-sheath and chitin-core nanowhiskers. Carbohydr Polym 107:158–166
37. Zhang Y, Xue C, Xue Y, Gao R, Zhang X (2005) Determination of the degree of deacetylation of chitin and chitosan by X-ray powder diffraction. Carbohydr Res 340:1914–1917
38. Bragg WH, Bragg WL (1913) The reflection of X-rays by crystals. Proc R Soc Lond Ser A 88:428–438
39. Azimi M, Peighambardoust SJ (2017) Methanol crossover and selectivity of nafion/hetero-polyacid/montmorillonite nanocomposite proton exchange membranes for DMFC Applications. Iran J Chem Eng (IJChE) 14:65–81
40. Kim D, Scibioh MA, Kwak S, Oh IH, Ha HY (2004) Nano-silica layered composite membranes prepared by PECVD for direct methanol fuel cells. Electrochem Commun 6:1069–1074
41. Hasanabadi N, Ghaffarian SR, Hasani-Sadrabadi MM (2011) Magnetic field aligned nanocomposite proton exchange membranes based on sulfonated poly (ether sulfone) and Fe_2O_3 nanoparticles for direct methanol fuel cell application. Int J Hydrog Energy 36:15323–15332
42. Zvezdova D (2010) Synthesis and characterization of chitosan from marine sources in Black Sea. Ann Proc 49:65–69 **("Angel Kanchev" University of Ruse)**
43. Hai TAP, Sugimoto R (2018) Surface modification of chitin and chitosan with poly (3-hexylthiophene) via oxidative polymerization. Appl Surf Sci 434:188–197
44. Li C, Liu H, Luo B, Wen W, He L, Liu M, Zhou C (2016) Nanocomposites of poly (*l*-lactide) and surface-modified chitin whiskers with improved mechanical properties and cytocompatibility. Eur Polym J 81:266–283
45. Li J, Revol JF, Marchessault R (1997) Effect of degree of deacetylation of chitin on the properties of chitin crystallites. J Appl Polym Sci 65:373–380
46. Tsai HS, Wang YZ, Lin JJ, Lien WF (2010) Preparation and properties of sulfopropyl chitosan derivatives with various sulfonation degree. J Appl Polym Sci 116:1686–1693
47. Jayakumar R, Nwe N, Nagagama H, Furuike T, Tamura H (2008) Synthesis, characterization and biospecific degradation behavior of sulfated chitin. Macromol Symp 1:163–167
48. Wang N, Ding E, Cheng R (2007) Thermal degradation behaviors of spherical cellulose nanocrystals with sulfate groups. Polymer 48:3486–3493
49. Kim D-Y, Nishiyama Y, Wada M, Kuga S (2001) High-yield carbonization of cellulose by sulfuric acid impregnation. Cellulose 8:29–33
50. Casadidio C, Peregrina DV, Gigliobianco MR, Deng S, Censi R, Di Martino P (2019) Chitin and chitosans: characteristics, eco-friendly processes, and applications in cosmetic science. Mar Drugs 17:369
51. Ioelovich M (2014) Crystallinity and hydrophility of chitin and chitosan. J Chem 3:7–14
52. Li Q, Zhou J, Zhang L (2009) Structure and properties of the nanocomposite films of chitosan reinforced with cellulose whiskers. J Polym Sci B 47:1069–1077
53. Tohidian M, Ghaffarian SR, Nouri M, Jaafarnia E, Haghighi AH (2015) Polyelectrolyte nanocomposite membranes using imidazole-functionalized nanosilica for fuel cell applications. J Macromol Sci B 54:17–31
54. Tohidian M, Ghaffarian SR (2018) Surface modified multi-walled carbon nanotubes and Nafion nanocomposite membranes for use in fuel cell applications. Polym Adv Technol 29:1219–1226

55. Marschall R, Sharifi M, Wark M (2009) Proton conductivity of imidazole functionalized ordered mesoporous silica: influence of type of anchorage, chain length and humidity. Microporous Mesoporous Mater 123:21–29
56. Haghighi AH, Tohidian M, Ghaderian A, Shakeri SE (2017) Polyelectrolyte nanocomposite membranes using surface modified nanosilica for fuel cell applications. J Macromol Sci B 56:383–394
57. Jiang Z, Zheng X, Wu H, Wang J, Wang Y (2008) Proton conducting CS/P (AA-AMPS) membrane with reduced methanol permeability for DMFCs. J Power Sources 180:143–153